Ultimate bounds for precision of atomic clock frequency measurement: Rabi, Ramsey, and coherent-population-trapping techniques

Stefano Olivares [1,*] Salvatore Micalizio [2,†] and Matteo G. A. Paris [1,‡]

[1] *Dipartimento di Fisica "Aldo Pontremoli," Università degli Studi di Milano and INFN Sezione di Milano, 20133 Milano, Italia*

[2] *Quantum Metrology and Nanotechnologies Division, Istituto Nazionale di Ricerca Metrologica, Strada delle Cacce 91, 10135 Torino, Italia*

(Received 1 September 2025; accepted 22 April 2026; published 13 May 2026)

We investigate the ultimate quantum limits to the achievable uncertainty in the estimation of the transition frequency between two atomic levels. We focus on Rabi, Ramsey, and coherent-population-trapping (CPT) techniques, which are widely employed in experiments. We prove that in the Rabi and Ramsey schemes, measuring the atomic population allows one to reach the minimum uncertainty, but for the CPT setup, a measurement involving the coherences between the levels results in a further improvement of the estimation. As a paradigmatic example of possible noises, the effect of cavity coupling fluctuations is considered in the Rabi and Ramsey scenarios. As a figure of merit, we assess the Fisher information of the population measurement and compare its value with the maximum one given by the quantum Fisher information, which is achieved by optimizing over all the possible measurements allowed by quantum mechanics.

DOI: 10.1103/gk6v-7ghm

I. INTRODUCTION

Estimating the frequency of an atomic transition is at the basis of a large variety of physical measurements, including frequency metrology [1,2], high-resolution spectroscopy [3], and possible time variation of the fundamental constants [4]. Several techniques have been developed to observe atomic transitions, particularly those characterized by a high signal-to-noise ratio and only partially influenced by broadening mechanisms. Moreover, to accurately determine the frequency of a transition with high precision, it must remain observable for an extended period, in accordance with the Heisenberg uncertainty principle. In this context, laser cooling techniques [5] have enabled the measurement of atomic clock frequencies with unprecedented accuracy, first using Cs or Rb fountains [6] and later with optical clocks [7].

The optimization of an atomic frequency measurement and the determination of the intrinsic precision bounds can be tackled at a more fundamental level by means of the estimation theory. Among the available unbiased estimators, the one with the smallest variance offers the highest precision of the estimate. In turn, a lower bound on the variance of any unbiased estimator may be defined by the Cramér-Rao inequality [8].

Specifically, to estimate the (angular) frequency $\omega_{\rm A}$ of a two-level atomic transition, we start from a sample of atoms prepared in one of the two levels. Then we let them interact with an oscillating electric field, and a signal proportional to the transition probability $p_{\omega_{\rm A}}(\omega)$ is maximized (or minimized) by changing the frequency ω of the applied field. This process leads to an estimate of $\omega_{\rm A}$ through a measurement of $p_{\omega_{\rm A}}(\omega)$. The framework of estimation theory imposes a bound on the uncertainty of the estimation of $\omega_{\rm A}$, that is, its variance, which in this case satisfies the inequality

$$\mathrm{var}(\omega_{\rm A}) \geqslant \left[\mathcal{M} F_{\omega_{\rm A}}(\omega)\right]^{-1}, \tag{1}$$

where $F_{\omega_{\rm A}}(\omega)$ is the Fisher information and $\mathcal{M}$ is the statistical scaling, that is, the number of measurement repetitions or outcomes [8]. Given that population measurement has only two possible outcomes, we have

$$F_{\omega_{\rm A}}(\omega) = \frac{\left[\partial_{\omega_{\rm A}} p_{\omega_{\rm A}}(\omega)\right]^2}{p_{\omega_{\rm A}}(\omega)\left[1 - p_{\omega_{\rm A}}(\omega)\right]}. \tag{2}$$

The transition probability depends on the specific technique adopted to excite and detect the atomic transition. It is then of interest to investigate how the Fisher information expressed by Eq. (2) changes accordingly.

In this paper we consider three techniques commonly used in atomic clock operation and investigate their fundamental limits: (i) the Rabi method, where the atoms interact with a single-mode electromagnetic field pulse; (ii) the Ramsey scheme, where the interaction is split into two Rabi-like interactions separated by a much longer noninteracting region; and (iii) the coherent-population-trapping (CPT) phenomenon where the atoms interact with two phase coherent fields coupling the two clock transition levels to a common excited state. For each technique, we will calculate the Fisher information and the corresponding quantum Fisher information [8–10], i.e., the Fisher information achievable with the same physical probe and optimizing over all possible measurement allowed

*Contact author: stefano.olivares@fisica.unimi.it

†Contact author: s.micalizio@inrim.it

‡Contact author: matteo.paris@fisica.unimi.it

by quantum mechanics. Moreover, since imperfections unavoidably affect the considered schemes, as a paradigmatic example we address the effect of cavity coupling fluctuations on our results in the case of the Rabi and Ramsey frameworks; in the CPT scenario the loss of coherence and spontaneous decay are instead embedded into the theoretical model from the beginning. We remark that our study is a theoretical investigation into the fundamental bounds to precision as set by quantum mechanics and is not related to the practical limitations, such as those connected with local oscillator noise or feedback loops.

In general, if $\hat{\rho} = \hat{\rho}(\lambda)$ is the density operator describing the state of the system under investigation and λ is the parameter we want to estimate, the minimum uncertainty is bounded by (we drop the statistical scaling factor)

$$\mathrm{var}_{\min}(\lambda) \geqslant [H(\lambda)]^{-1}, \tag{3}$$

where $H(\lambda)$ is the quantum Fisher information [9]

$$H(\lambda) = \mathrm{Tr}\big(\hat{\rho}\hat{\mathcal{L}}_\lambda^2\big), \tag{4}$$

where we introduced $\hat{\mathcal{L}}_\lambda$, the symmetric logarithmic derivative, such that

$$\hat{\mathcal{L}}_\lambda\hat{\rho} + \hat{\rho}\hat{\mathcal{L}}_\lambda = 2\partial_\lambda\hat{\rho}. \tag{5}$$

If we write $\hat{\rho} = \sum_n r_n |\psi_n\rangle\langle\psi_n|$, with $\{|\psi_n\rangle\}$ the eigenbasis of $\hat{\rho}$ and $\{r_n\}$ the corresponding eigenvalues, we have

$$H(\lambda) = 2\sum_{n,m} \frac{|\langle\psi_n|(\partial_\lambda\hat{\rho})|\psi_m\rangle|^2}{r_n + r_m}, \tag{6}$$

where the sum includes only the terms with $r_n + r_m \neq 0$.

In the following, we show that estimation strategies based on the considered Rabi, Ramsey, and CPT techniques allow one to achieve the ultimate limits to precision imposed by quantum mechanics since, at resonance, the corresponding Fisher and quantum Fisher information coincide. Our approach based on estimation and quantum estimation theory leads us to prove that the Ramsey method beats both the Rabi and the CPT performance, as also suggested by the results of current experiments [1,2]. Interestingly, when a measurement involving the coherence between the levels is considered, we find that for the coherent population trapping, the Fisher and the quantum Fisher information are only slightly different for any value of the detuning $\Delta\omega = \omega_\mathrm{A} - \omega$ and coincide at resonance; however, for the Rabi and Ramsey methods, the quantum Fisher information is sensibly higher than the classical information for nonzero values of $\Delta\omega$, thus fostering new investigation for different detection schemes allowing one to reach that limit.

The paper is organized as follows. Section II introduces the Rabi (Sec. II A) and Ramsey (Sec. II B) schemes for the estimation of the atomic transition frequency together with the corresponding Fisher information and their quantum counterparts. Here we also address how these results are affected by fluctuations of the cavity interaction couplings (Sec. II C), while the possible comparison with typical experiments is discussed in Sec. II D. The fundamental bounds of the CPT technique are investigated in Sec. III. We summarize our work and discuss our findings in Sec. IV.

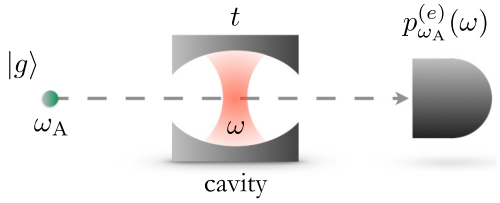

FIG. 1. Scheme of the Rabi method.

II. RABI AND RAMSEY APPROACHES

A. Rabi method

Initially conceived for measuring nuclear magnetic moments [11], the Rabi resonance method soon became a relevant tool to investigate atomic spectra with high resolution. In this technique, the atoms interact with a single laser or microwave pulse, depending on the frequency of the transition considered. Observing the atoms' absorption as a function of the local oscillator frequency results in a discriminant curve that carries the information about the atomic resonance frequency. Rabi excitation is nowadays very often used in optical frequency standards [7] because of its experimental simplicity compared to the Ramsey approach, as we will see later.

The scheme of the Rabi method is sketched in Fig. 1. A two-level atom, initially prepared in its ground state $|g\rangle$, interacts with an oscillating electric field inside a cavity for a time t. At resonance, i.e., when ω is equal to the atomic transition frequency ω_A, if the interaction time is set to $t = \pi/\Omega_0$ (that is, in the presence of a π pulse), with Ω_0 the Rabi frequency, the atom is finally found in the excited state $|e\rangle$ with certainty. However, in the presence of a detuning $\Delta\omega = \omega_\mathrm{A} - \omega$, the π pulse brings the atom to its excited state with probability (see Appendix A for details of the calculations)

$$p^{(e)}_{\omega_\mathrm{A}}(\omega) = \frac{1}{[\Theta_{\Omega_0}(\Delta\omega)]^2}\sin^2\left(\frac{\pi}{2}\Theta_{\Omega_0}(\Delta\omega)\right), \tag{7}$$

with

$$\Theta_{\Omega_0}(\Delta\omega) = \sqrt{1 + \left(\frac{\Delta\omega}{\Omega_0}\right)^2}, \tag{8}$$

which is plotted in Fig. 2(a) as a function of $\Delta\omega/\Omega_0$.

It is clear that the maximum $p^{(e)}_{\omega_\mathrm{A}}$ is attained at $\Delta\omega = 0$ and thus we can use $p^{(e)}_{\omega_\mathrm{A}}$ to estimate the atomic transition frequency. In this case, the uncertainty of the estimation of ω_A, that is, its variance, satisfies the inequality (we drop the statistical scaling factor)

$$\mathrm{var}(\omega_\mathrm{A}) \geqslant \frac{1}{F^{(\mathrm{Rbi})}_{\omega_\mathrm{A}}(\omega_\mathrm{A})}, \tag{9}$$

where the $F^{(\mathrm{Rbi})}_{\omega_\mathrm{A}}(\omega_\mathrm{A})$ is the Fisher information [8], namely,

$$F^{(\mathrm{Rbi})}_{\omega_\mathrm{A}}(\omega) = \sum_{k=g,e} p^{(k)}_{\omega_\mathrm{A}}(\omega)\big\{\partial_{\omega_\mathrm{A}}\ln\big[p^{(k)}_{\omega_\mathrm{A}}(\omega)\big]\big\}^2 \tag{10}$$

$$= \frac{\big[\partial_{\omega_\mathrm{A}}p^{(e)}_{\omega_\mathrm{A}}(\omega)\big]^2}{p^{(e)}_{\omega_\mathrm{A}}(\omega)\big[1 - p^{(e)}_{\omega_\mathrm{A}}(\omega)\big]}, \tag{11}$$

with $p^{(g)}_{\omega_\mathrm{A}}(\omega) = 1 - p^{(e)}_{\omega_\mathrm{A}}(\omega)$ the probability to detect the ground state of the atom after the interaction with the cavity.

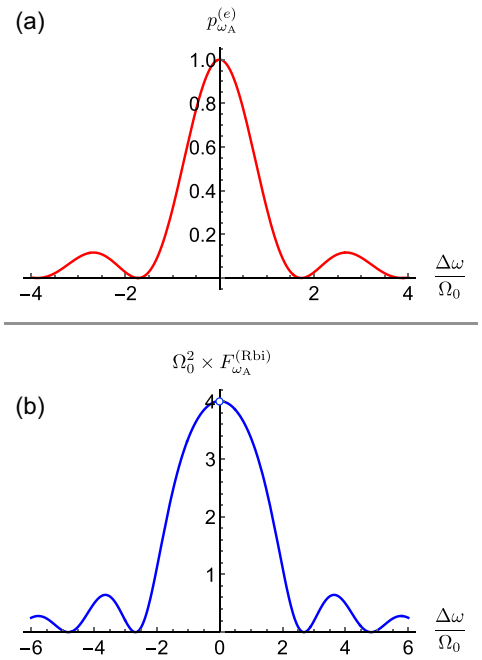

FIG. 2. (a) Plot of the Rabi probability $p^{(e)}_{\omega_A}$ to find the atom in the excited state after the interaction with the cavity as a function of $\Delta\omega/\Omega_0$. The atom is initially in the ground state and the interaction time corresponds to a π pulse. (b) Plot of the Fisher information $F^{(\mathrm{Rbi})}_{\omega_A}$ associated with the Rabi method as a function of $\Delta\omega/\Omega_0$. Note that at $\omega = \omega_A$ the Cramér-Rao theorem does not apply; see the text for details.

It is worth noting that at $\omega = \omega_A$ the statistical model changes rank (we only have one non-null element, namely, the atoms are always found in their excited state) and the Cramér-Rao theorem does not hold.

The analytical expression of $F^{(\mathrm{Rbi})}_{\omega_A}(\omega)$ is quite clumsy and it is not reported here explicitly. We illustrate its behavior in Fig. 2(b) as a function of $\Delta\omega/\Omega_0$. If $\omega \approx \omega_A$, the following expansion holds:

$$F^{(\mathrm{Rbi})}_{\omega_A}(\omega) \approx \frac{1}{\Omega_0^2}\left[4 - \left(8 - \frac{3}{4}\pi^2\right)\left(\frac{\omega - \omega_A}{\Omega_0}\right)^2\right]. \tag{12}$$

By explicitly evaluating Eq. (6) in the presence of the corresponding evolved state (see Appendix A for details), we can retrieve the quantum Fisher information, which is reported in Fig. 3. We note that for $\Delta\omega = 0$ the values of the Fisher and of the quantum Fisher information are the same: In this regime the atomic population measurement turns out to be optimal. However, we can also see that for $\Delta\omega \neq 0$ the quantum Fisher information may be greater than the classical information obtained from the atomic population detection.

B. Ramsey method

The atomic resonance can be also probed by the Ramsey method of separated fields where the atoms interact with two phase coherent laser or microwave pulses separated by a dark interval [12]. Compared to the Rabi method, the Ramsey excitation provides a narrower Fourier-limited linewidth for the same interrogation time. The atomic resonance frequency is then determined with a higher resolution. For atomic clock

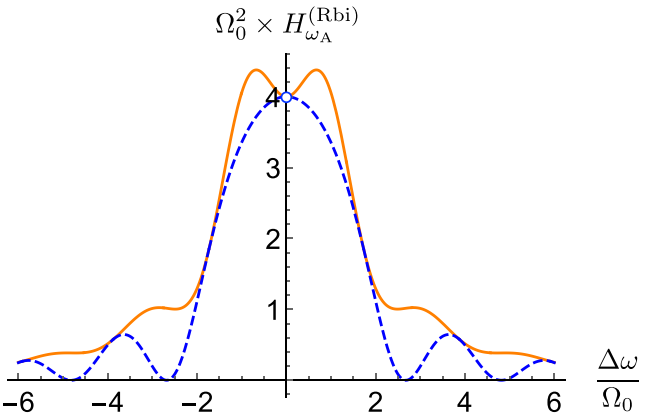

FIG. 3. Plot of the quantum Fisher information $H^{(\mathrm{Rbi})}_{\omega_A}$ associated with the Rabi method (orange solid line) as a function of $\Delta\omega/\Omega_0$. The blue dashed line is the Fisher information of Fig. 2(b).

applications, the Ramsey technique was first introduced in Cs beam tubes [13], then in cold-atom fountains (see [6] and reference therein), and more recently also in vapor cell arrangements [14–17].

The scheme of the Ramsey method is reported in Fig. 4. With respect to the Rabi scheme addressed in the preceding section, now, after the interaction with a first cavity, the atom undergoes a free evolution for a time T and then it interacts with a second cavity before the final measurement. Without loss of generality, we can set $T = \kappa\tau$. The interaction time is set to $\tau = \pi/2\Omega_0$ for both cavities (note that if $T \to 0$ we recover the Rabi scheme), and, after the whole evolution, the probability to find the atom in the excited state reads (see Appendix B for the derivation)

$$\begin{aligned} P^{(e)}_{\omega_A}(\omega;\kappa) = {} & \frac{4}{[\Theta_{\Omega_0}(\Delta\omega)]^2}\sin^2\left(\frac{\pi}{4}\Theta_{\Omega_0}(\Delta\omega)\right) \\ & \times\left[\cos\left(\frac{\kappa\Delta\omega}{4\Omega_0}\right)\cos\left(\frac{\pi}{4}\Theta_{\Omega_0}(\Delta\omega)\right) - \frac{\Delta\omega/\Omega_0}{\Theta_{\Omega_0}(\Delta\omega)}\right. \\ & \left.\times\sin\left(\frac{\kappa\Delta\omega}{4\Omega_0}\right)\sin\left(\frac{\pi}{4}\Theta_{\Omega_0}(\Delta\omega)\right)\right]^2, \end{aligned} \tag{13}$$

where $\Theta_{\Omega_0}(\Delta\omega)$ is still given by Eq. (8).

In Fig. 5 we plot $P^{(e)}_{\omega_A}$ for two different values of T. The typical Ramsey interference fringes are evident and the longer the free-evolution time T between the cavities, the larger the number of peaks. For comparison, in the same figure we plot $p^{(e)}_{\omega_A}$ (green dashed lines).

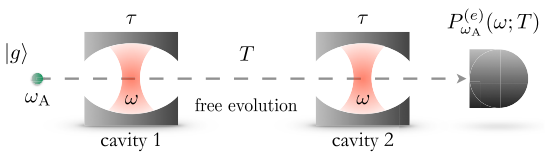

FIG. 4. Scheme of the Ramsey method.

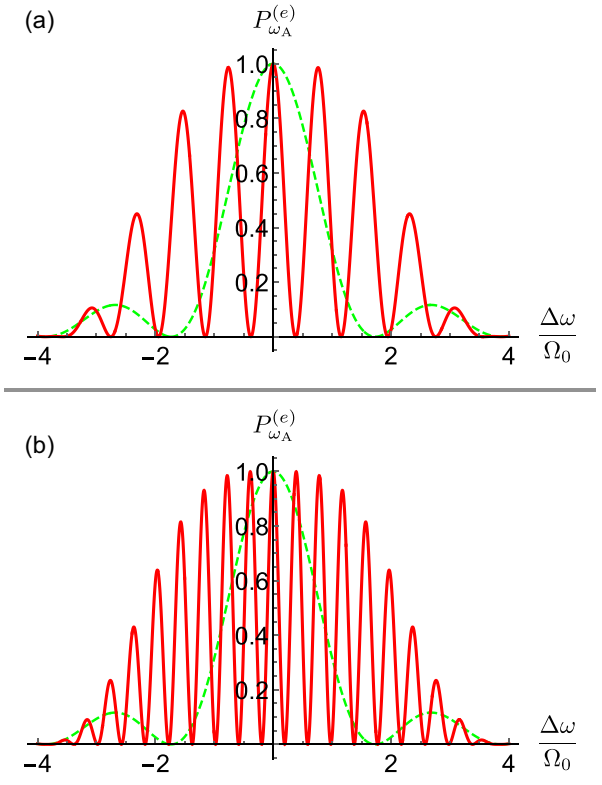

FIG. 5. Probability $P^{(e)}_{\omega_A}$ to find the atom in the excited state after the whole evolution as a function of $\Delta\omega/\Omega_0$ (red solid lines). The atom is initially in the ground state and the interaction time τ with the cavity field corresponds to a $\pi/2$ pulse. We set (a) $\kappa = 5$ and (b) $\kappa = 10$ for the free-evolution time $T = \kappa\,\tau$. The green dashed lines refer to $p^{(e)}_{\omega_A}$ given in Fig. 2.

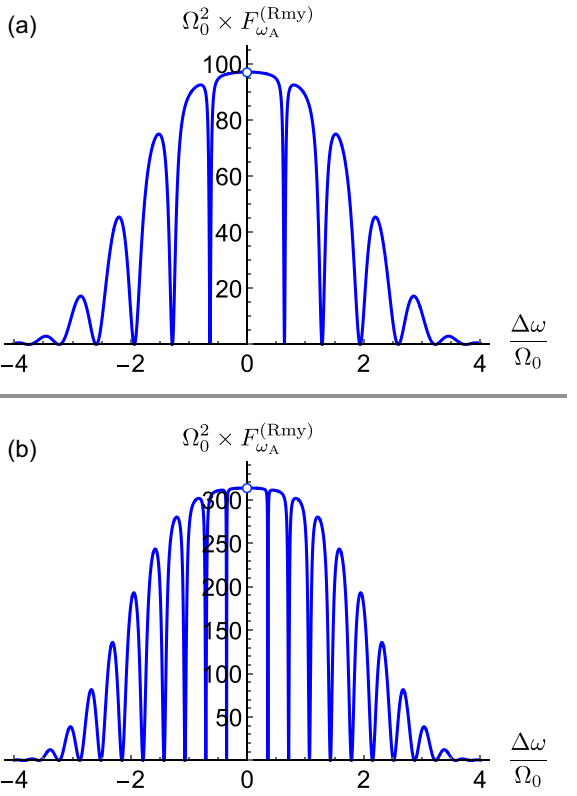

FIG. 6. Plot of the Fisher information $F^{(\mathrm{Rmy})}_{\omega_A}$ associated with the Ramsey method as a function of $\Delta\omega/\Omega_0$. The maximum is achieved at $\omega = \omega_A$. We set (a) $\kappa = 5$ and (b) $\kappa = 10$ for the free-evolution time $T = \kappa\,\tau$. As in the Rabi method, at $\omega = \omega_A$, the Cramér-Rao theorem does not apply; see the text for details.

Since the width of the peak of $P^{(e)}_{\omega_A}$ at $\omega = \omega_A$ is smaller than the one of $p^{(e)}_{\omega_A}$, we also expect the Fisher information

$$F^{(\mathrm{Rmy})}_{\omega_A}(\omega) = \sum_{k=g,e} P^{(k)}_{\omega_A}(\omega;\kappa)\left\{\partial_{\omega_A} \ln\left[P^{(k)}_{\omega_A}(\omega;\kappa)\right]\right\}^2 \quad (14)$$

$$= \frac{\left[\partial_{\omega_A} P^{(e)}_{\omega_A}(\omega)\right]^2}{P^{(e)}_{\omega_A}(\omega)\left[1 - P^{(e)}_{\omega_A}(\omega)\right]} \quad (15)$$

to be larger. Now the analytic expression of $F^{(\mathrm{Rmy})}_{\omega_A}(\omega)$ is clumsy and it is not reported here explicitly, but it is plotted in Fig. 6 for the same values of T chosen in Fig. 5. As for the Rabi method, also in the case of the Ramsey method the rank of the statistical model changes at $\omega = \omega_A$ and the Cramér-Rao theorem is not applicable.

We can see that the maximum of the Fisher information is still attained at $\omega = \omega_A$. If $\omega \approx \omega_A$, we find the expansion

$$F^{(\mathrm{Rmy})}_{\omega_A}(\omega) \approx \frac{1}{\Omega_0^2}\left[4\left(1 + \frac{\pi}{4}\kappa\right)^2 - \left(8 - \frac{3}{4}\pi^2 + (10 - 3\pi)\frac{\pi}{2}\kappa\right)\left(\frac{\omega - \omega_A}{\Omega_0}\right)^2\right]. \quad (16)$$

Note that for $\kappa = 0$, $F^{(\mathrm{Rmy})}_{\omega_A}(\omega)$ reduces to $F^{(\mathrm{Rbi})}_{\omega_A}(\omega)$ in Eq. (12). Remarkably, if the free-evolution time $T = \kappa\tau$ is much longer than the in-cavity interaction time τ, namely, $\kappa \gg 1$, Eq. (16) reduces to (still for $\omega \approx \omega_A$)

$$F^{(\mathrm{Rmy})}_{\omega_A}(\omega) \approx \frac{4}{\Omega_0^2}\left(1 + \frac{\pi}{4}\kappa\right)^2, \quad (17)$$

which is independent of ω. It is also worth noting that, in the correspondence of the maximum ($\omega = \omega_A$), the ratio between the Fisher information in the case of the Ramsey and Rabi methods scales as

$$\frac{F^{(\mathrm{Rmy})}_{\omega_A}(\omega_A)}{F^{(\mathrm{Rbi})}_{\omega_A}(\omega_A)} = \left(1 + \frac{\pi}{4}\kappa\right)^2. \quad (18)$$

The quantum information associated with the Ramsey measurement follows from Eq. (6) with the corresponding evolved state (see Appendix B for details). The result is shown in Fig. 7. As in the case of the Rabi configuration, when $\Delta\omega = 0$ the Fisher and the quantum Fisher information exhibit the same value, underlying that the population measurement is still optimal. Nevertheless, we still find that there are intervals with $\Delta\omega \neq 0$ for which the quantum Fisher information may be greater than the classical information attained due to the atomic population detection.

C. Effect of cavity coupling fluctuations

There are many imperfections that can affect the evolution of the atoms throughout the whole setup. Since the dissipative

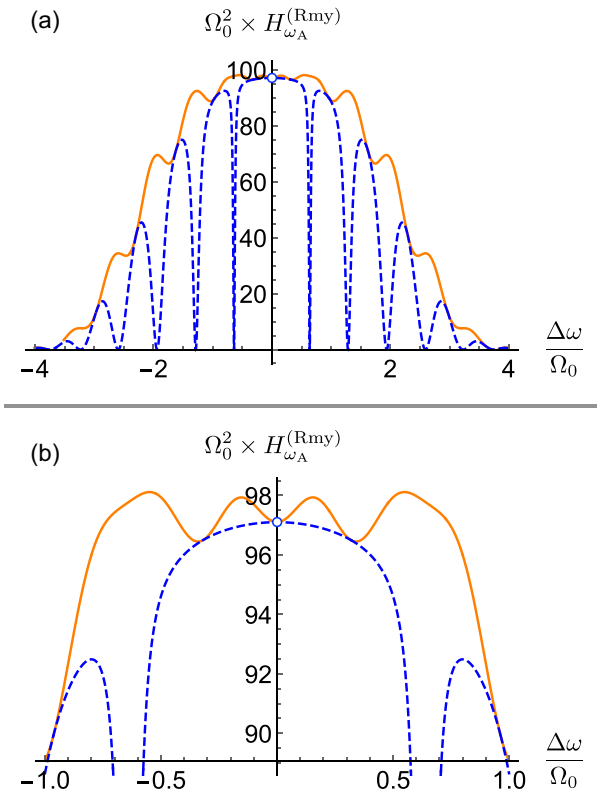

FIG. 7. (a) Plot of the quantum Fisher information $H_{\omega_A}^{(\mathrm{Rmy})}$ associated with the Ramsey method (orange solid line) as a function of $\Delta\omega/\Omega_0$. The blue dashed line is the Fisher information of Fig. 6. We set $\kappa = 5$ for the free-evolution time $T = \kappa\,\tau$. (b) Magnification of the top plot.

effect is negligible (in experiments the two hyperfine levels of the ground state are considered), we can focus on nondissipative effects. This kind of fluctuations may arise from the presence of coupling fluctuations, but similar results can be obtained in the velocity spread of the atomic sample (in the considered scenarios the interaction time depends on the actual velocity of the atoms) [18].

Here we are not interested in providing a full analysis of how the possible imperfections affect the actual implementations, thus we introduce a simple effective model that takes into account coupling fluctuations within the cavities [19].

We assume that the Rabi frequencies introduced above fluctuate around their mean values Ω_0, namely,

$$\Omega_0 \to \Omega_0(1+\zeta), \tag{19}$$

where $\zeta = \delta\Omega_0/\Omega_0$ can be seen as a mean-zero stochastic variable with suitable distribution. In the following, for the sake of simplicity and clarity, we assume that ζ is distributed according to a normal distribution.

Thereafter, in the case of the Rabi scheme, the statistical model describing the evolved atomic state can be written as

$$\overline{\varrho}_{\omega_A}^{(\mathrm{Rbi})}(t) = \int_{\mathbb{R}} \mathrm{d}\zeta\, \frac{\mathrm{e}^{-\zeta^2/(2\sigma^2)}}{\sqrt{2\pi\sigma^2}}\, \varrho_{\omega_A|\zeta}^{(\mathrm{Rbi})}(t), \tag{20}$$

where

$$\varrho_{\omega_A|\zeta}^{(\mathrm{Rbi})}(t) = |\psi_\zeta(t)\rangle\langle\psi_\zeta(t)|, \tag{21}$$

with

$$|\psi_\zeta(t)\rangle = \tilde{U}(\Omega_0(1+\zeta);t)|g\rangle, \tag{22}$$

where $\tilde{U}$ is given in Eqs. (A7).

In the Ramsey scheme the two cavities may exhibit Rabi frequencies that fluctuates independently. The corresponding statistical model leads to the density operator

$$\overline{\varrho}_{\omega_A}^{(\mathrm{Rmy})}(\tau,T) = \int_{\mathbb{R}^2} \mathrm{d}\zeta_1\,\mathrm{d}\zeta_2\, \frac{\mathrm{e}^{-\zeta_1^2/(2\sigma_1^2)}}{\sqrt{2\pi\sigma_1^2}}\, \frac{\mathrm{e}^{-\zeta_2^2/(2\sigma_2^2)}}{\sqrt{2\pi\sigma_2^2}}\, \varrho_{\omega_A|\zeta_1;\zeta_2}^{(\mathrm{Rmy})}(\tau,T), \tag{23}$$

and now

$$\varrho_{\omega_A|\zeta_1;\zeta_2}^{(\mathrm{Rmy})}(\tau,T) = \big|\Psi_{\zeta_1;\zeta_2}(\tau,T)\big\rangle\big\langle\Psi_{\zeta_1;\zeta_2}(\tau,T)\big|, \tag{24}$$

with

$$|\Psi_{\zeta_1;\zeta_2}(\tau,T)\rangle = \tilde{U}(\Omega_0(1+\zeta_1);\tau)\tilde{U}_{\mathrm{free}}(T)\tilde{U}(\Omega_0(1+\zeta_2);\tau)|g\rangle, \tag{25}$$

where $\tilde{U}$ is still given in Eqs. (A7), while $\tilde{U}_{\mathrm{free}}$ is in Eqs. (B1). For the sake of simplicity, in the following analysis we set $\sigma_1 = \sigma_2 = \sigma$.

Accordingly, the probabilities of finding an atom in the excited state after the evolution are (we still assume that $\Omega_0 t = \pi$ and $\Omega_0\tau = \pi/2$)

$$\overline{p}_{\omega_A}^{(e)}(\omega) = \langle e|\overline{\varrho}_{\omega_A}^{(\mathrm{Rbi})}(t = \pi/\Omega_0)|e\rangle \tag{26}$$

and

$$\overline{P}_{\omega_A}^{(e)}(\omega) = \langle e|\overline{\varrho}_{\omega_A}^{(\mathrm{Rmy})}(\tau = \pi/2\Omega_0)|e\rangle, \tag{27}$$

respectively, and one can (numerically) evaluate the corresponding Fisher information

$$\overline{F}_{\omega_A}^{(\mathrm{Rbi})}(\omega) = \frac{\big[\partial_{\omega_A}\overline{p}_{\omega_A}^{(e)}(\omega)\big]^2}{\overline{p}_{\omega_A}^{(e)}(\omega)\big[1-\overline{p}_{\omega_A}^{(e)}(\omega)\big]} \tag{28}$$

and

$$\overline{F}_{\omega_A}^{(\mathrm{Rmy})}(\omega) = \frac{\big[\partial_{\omega_A}\overline{P}_{\omega_A}^{(e)}(\omega)\big]^2}{\overline{P}_{\omega_A}^{(e)}(\omega)\big[1-\overline{P}_{\omega_A}^{(e)}(\omega)\big]}. \tag{29}$$

To calculate the quantum Fisher information associated with a density operator $\hat{\rho}_\lambda$, we can use the relation [20]

$$H(\lambda) = 8\lim_{\varepsilon\to 0} \frac{1-\mathrm{Tr}(\sqrt{\sqrt{\hat{\rho}_\lambda}\hat{\rho}_{\lambda+\varepsilon}\sqrt{\hat{\rho}_\lambda}})}{\varepsilon^2}, \tag{30}$$

which allows us to numerically evaluate $\overline{H}_{\omega_A}^{(\mathrm{Rbi})}$ and $\overline{H}_{\omega_A}^{(\mathrm{Rmy})}$. The results are shown in Figs. 8 and 9.

It is worth noting that now the Fisher information goes to zero as $\Delta\omega \to 0$. This result can be explained by investigating the mathematical definition of the Fisher information. As in the noiseless case, we have $\partial_{\omega_A} p_{\omega_A}^{(e)}, \partial_{\omega_A} P_{\omega_A}^{(e)} = 0$ for $\Delta\omega = 0$ but now $p_{\omega_A}^{(e)}, P_{\omega_A}^{(e)} < 1$ (see Fig. 10); therefore, the statistical model is well defined and the ratio in Eqs. (28) and (29) goes to zero. Analogous behaviors can be found also investigating other scenarios, as in quantum interferometry [21]. A similar result arises when the excitation rates of Rabi and Ramsey

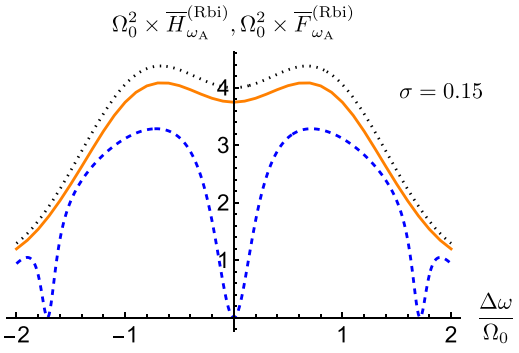

FIG. 8. Plot of the quantum Fisher information $\overline{H}^{(\mathrm{Rbi})}_{\omega_\mathrm{A}}$ (orange solid line) and the Fisher information $\overline{F}^{(\mathrm{Rbi})}_{\omega_\mathrm{A}}$ (blue dashed line) as a function of the ratio $\Delta\omega/\Omega_0$ in the case of the Rabi method for $\sigma = 0.15$, characterizing the coupling fluctuations. For comparison, we also plot the quantum Fisher information in the noiseless case (black dotted line). Note that for $\Delta\omega = 0$ now we have $\overline{F}^{(\mathrm{Rbi})}_{\omega_\mathrm{A}} = 0$. See the text for details.

spectra do not reach 1 due to temperature effect, spontaneous emission, Raman scattering between atoms and light, and so on [22].

We note that, by postprocessing the data, it is possible to renormalize the probabilities $\overline{p}^{(e)}_{\omega_\mathrm{A}}(\omega)$ and $\overline{P}^{(e)}_{\omega_\mathrm{A}}(\omega)$ with respect to the known and fixed quantities $\overline{p}^{(e)}_{\omega_\mathrm{A}}(\omega_\mathrm{A})$ and $\overline{P}^{(e)}_{\omega_\mathrm{A}}(\omega_\mathrm{A})$, namely,

$$\tilde{p}^{(e)}_{\omega_\mathrm{A}}(\omega) = \frac{\overline{p}^{(e)}_{\omega_\mathrm{A}}(\omega)}{\overline{p}^{(e)}_{\omega_\mathrm{A}}(\omega_\mathrm{A})}, \quad \tilde{P}^{(e)}_{\omega_\mathrm{A}}(\omega) = \frac{\overline{P}^{(e)}_{\omega_\mathrm{A}}(\omega)}{\overline{P}^{(e)}_{\omega_\mathrm{A}}(\omega_\mathrm{A})}. \tag{31}$$

Thereafter, $\tilde{p}^{(e)}_{\omega_\mathrm{A}}(\omega_\mathrm{A}) = \tilde{P}^{(e)}_{\omega_\mathrm{A}}(\omega_\mathrm{A}) = 1$ and $\partial_{\omega_\mathrm{A}}\tilde{p}^{(e)}_{\omega_\mathrm{A}}(\omega_\mathrm{A}) = \partial_{\omega_\mathrm{A}}\tilde{P}^{(e)}_{\omega_\mathrm{A}}(\omega_\mathrm{A}) = 0$. The Fisher information calculated with the renormalized probabilities can be written as

$$\tilde{F}^{(\mathrm{Rbi})}_{\omega_\mathrm{A}}(\omega) = \frac{\left[\partial_{\omega_\mathrm{A}}\overline{p}^{(e)}_{\omega_\mathrm{A}}(\omega)\right]^2}{\overline{p}^{(e)}_{\omega_\mathrm{A}}(\omega)\left[\overline{p}^{(e)}_{\omega_\mathrm{A}}(\omega_\mathrm{A}) - \overline{p}^{(e)}_{\omega_\mathrm{A}}(\omega)\right]} \tag{32}$$

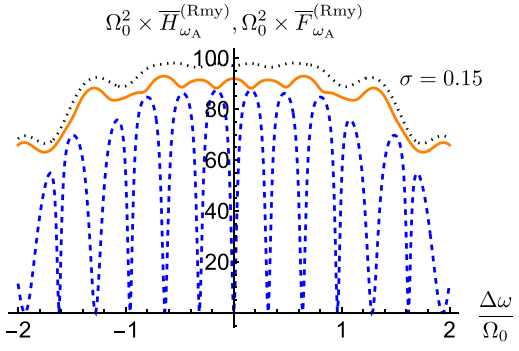

FIG. 9. Plot of the quantum Fisher information $\overline{H}^{(\mathrm{Rmy})}_{\omega_\mathrm{A}}$ (orange solid line) and the Fisher information $\overline{F}^{(\mathrm{Rmy})}_{\omega_\mathrm{A}}$ (blue dashed line) as a function of the ratio $\Delta\omega/\Omega_0$ in the case of the Ramsey method with $\kappa = 5$ and for $\sigma = 0.15$, characterizing the coupling fluctuations. For comparison, we also plot the quantum Fisher information in the absence of velocity fluctuations (black dotted line). Note that for $\Delta\omega = 0$ now we have $\overline{F}^{(\mathrm{Rbi})}_{\omega_\mathrm{A}} = 0$. See the text for details.

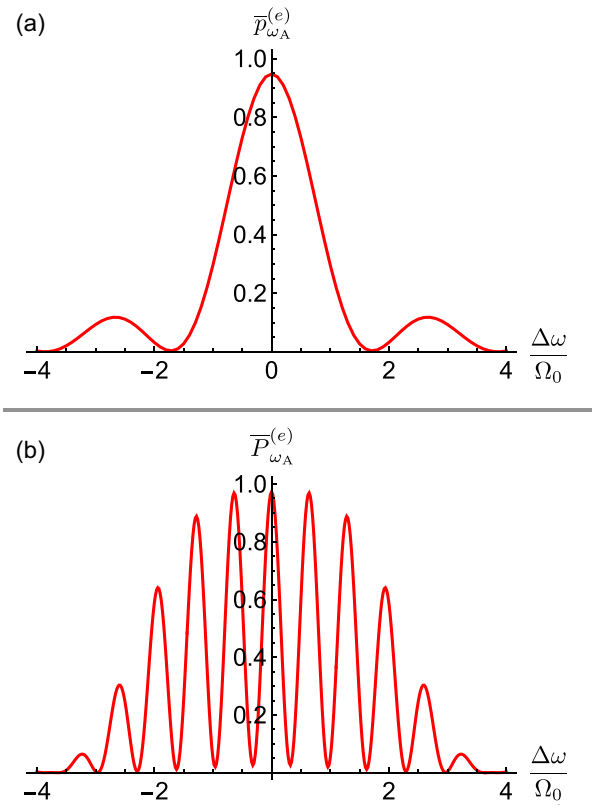

FIG. 10. Plot of the probabilities $\overline{p}^{(e)}_{\omega_\mathrm{A}}$ and $\overline{P}^{(e)}_{\omega_\mathrm{A}}$ as a function of the ratio $\Delta\omega/\Omega_0$ in the case of (a) the Rabi method and (b) the Ramsey method with $\kappa = 5$. In both the panels we set $\sigma = 0.15$. Note that for $\Delta\omega \to 0$ we find $\overline{p}^{(e)}_{\omega_\mathrm{A}}, \overline{P}^{(e)}_{\omega_\mathrm{A}} < 1$.

and

$$\tilde{F}^{(\mathrm{Rmy})}_{\omega_\mathrm{A}}(\omega) = \frac{\left[\partial_{\omega_\mathrm{A}}\overline{P}^{(e)}_{\omega_\mathrm{A}}(\omega)\right]^2}{\overline{P}^{(e)}_{\omega_\mathrm{A}}(\omega)\left[\overline{P}^{(e)}_{\omega_\mathrm{A}}(\omega_\mathrm{A}) - \overline{P}^{(e)}_{\omega_\mathrm{A}}(\omega)\right]}, \tag{33}$$

respectively, and are plotted in Fig. 11.

D. Comparison with experiments

Though we are interested in the theoretical fundamental limits of frequency estimation, we can provide a comparison with some experimental result concerning the investigation of atomic transitions as well as the atomic clocks.

Cesium beam clocks, atomic fountains, and optical clocks represent three generations of atomic timekeeping, each with increasing levels of precision. Cesium beam clocks, the earliest standard, use a beam of cesium atoms and microwave radiation to define the SI second based on the hyperfine transition frequency of cesium-133 [2]. Atomic fountains improve on this by cooling atoms with lasers and launching them upward, allowing for longer interaction times and thus greater accuracy [6]. Both cesium beam clocks and atomic fountains operate using the Ramsey technique of separated oscillatory fields. Optical clocks, the most advanced, employ optical (rather than microwave) transitions in atoms or ions, such as strontium or ytterbium, and benefit from much higher frequencies, leading to unprecedented time resolution [7]. The stability of these clocks is often analyzed using the Allan

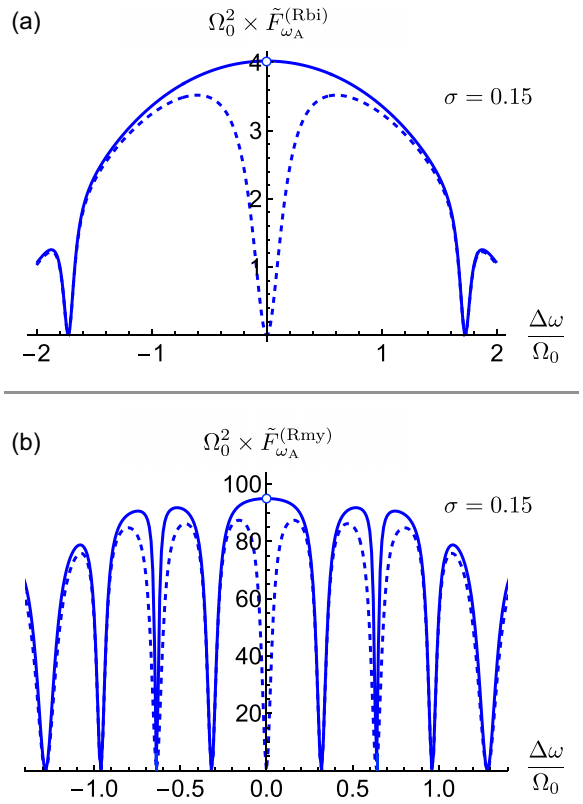

FIG. 11. Plot of the Fisher information $\tilde{F}$ (blue solid line) obtained by normalizing the probability (see the text for details) as a function of the ratio $\Delta\omega/\Omega_0$ in the case of (a) the Rabi method and (b) the Ramsey method with $\kappa = 5$ for $\sigma = 0.15$. We can see that the Fisher information again approaches $\Delta\omega = 0$ (now, at resonance, the statistical model is no longer well defined as it happens in the lossless scenario). For comparison, we also report the Fisher information without rescaling (blue dashed lines; see also Figs. 8 and 9).

variance [23], a statistical tool that quantifies frequency stability over time and reveals noise processes that can affect long-term precision.

In order to compare the results obtained in this study with the traditional tool of Allan variance, we begin by considering that the frequency stability of an atomic clock is conventionally characterized by the Allan deviation evaluated at an integration time of 1 s [23]. Therefore, we consider in Eq. (1) a sufficient number of averages to ensure that the Allan deviation at 1 s is estimated with a 10% uncertainty.

We start by considering the Ramsey approach applied to an atomic fountain; in the limit $\omega \to \omega_A$, due to Eqs. (1) and (16), we can estimate the (ultimate) fractional statistical fluctuations as

$$\frac{\delta\omega_A}{\omega_A} = \frac{1}{\sqrt{N_{at}M}} \frac{1}{\omega_A} \left[F^{(\mathrm{Rmy})}_{\omega_A}(\omega_A)\right]^{-1/2} \tag{34}$$

$$= \frac{1}{\sqrt{N_{at}M}} \frac{2\Omega_0}{\omega_A} \left(\frac{1}{4+\kappa\pi}\right), \tag{35}$$

where the factor $(N_{at}\,M)^{-1/2}$ accounts for the statistical scaling, related to the quantity $\mathcal{M}$ in Eq. (1), with N_{at} the total number of measured atom and M the number of averages. In typical fountain experiments involving cesium atoms one has (see, for example, Ref. [24]) $\omega_A^{Cs} = 2\pi \times 9.2$ GHz, $\Omega_0 \approx 350\ \mathrm{s}^{-1}$, $\kappa \approx 10^2$, $M \approx 100$, and $N_{at} \approx 10^6$, leading to

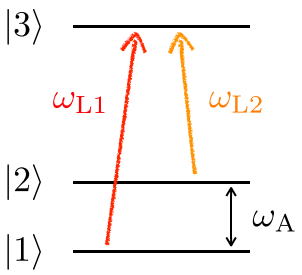

FIG. 12. Three-level system interacting with a couple of phase-coherent laser fields in a Λ scheme: ω_{L1} and ω_{L2} are the (angluar) frequencies of the lasers that couple levels $|1\rangle$ and $|3\rangle$ and levels $|2\rangle$ and $|3\rangle$, respectively.

$$\frac{\delta\omega_A^{Cs}}{\omega_A^{Cs}} \approx 10^{-14}. \tag{36}$$

Optical clocks operate based on a Rabi interrogation scheme, in which a coherent laser field drives a transition between two atomic energy levels over a well-defined interaction time. Considering a sample of ytterbium atoms (see, for instance, Ref. [25]), we have $\omega_A^{Yb} = 2\pi \times 518$ THz, $\Omega_0 \approx 10^2\ \mathrm{s}^{-1}$, $M \approx 100$, and $N_{at} \approx 5\times10^3$, and Eq. (12) yields

$$\frac{\delta\omega_A^{Yb}}{\omega_A^{Yb}} \approx 5\times10^{-18}. \tag{37}$$

The values expressed by Eqs. (36) and (37) represent the limits to the achievable statistical uncertainties in a clock frequency measurement considering the population measurement. These estimates are an order of magnitude lower than the experimental results, as in both cases the stability is limited not by statistics but by the noise of the local oscillator (microwave or laser, respectively) that is transferred onto the atomic transition. We still notice that the present analysis does not concern the accuracy of atomic clocks, which is defined by the evaluation and correction of systematic frequency shifts affecting the atomic transition.

III. COHERENT-POPULATION-TRAPPING APPROACH

Coherent population trapping is a quantum phenomenon in which two metastable levels (which usually are the two sublevels of the ground state defining the clock transition) are coupled to a common excited state through two phase-coherent laser fields [26], as shown in Fig. 12.

The trapping is made evident when the laser frequency difference $\omega_{L1} - \omega_{L2}$ matches the atomic frequency ω_A, the so-called Raman resonance condition. In this case, the atomic population is trapped in a coherent superposition of the two clock levels; the atoms are no longer able to absorb photons from the laser fields and consequently the fluorescence signal appears strongly reduced (dark line) [27–29]. For frequency standards applications, coherent population trapping has been implemented in cold-atom setups but above all in vapor cell clocks using hot atoms. While CPT is not currently used in the best optical clocks, it is widely employed in compact

atomic clocks [30,31] also for possible satellite applications and emerging quantum technologies. A thorough quantum-limited analysis of coherent population trapping is still lacking and we aim at providing a reference for future studies in quantum metrology.

With a density-matrix approach, it is possible to evaluate the atomic populations and the coherence generated by the CPT phenomenon in the ground state. The Hamiltonian of the system can be written in the matrix form as

$$\mathcal{H}_{\rm CPT} = \hbar \begin{pmatrix} \omega_1 & 0 & \Omega_{\rm R1} \\ 0 & \omega_2 & \Omega_{\rm R2} \\ \Omega_{\rm R1} & \Omega_{\rm R2} & \omega_3 \end{pmatrix}, \tag{38}$$

where ω_k is the frequency associated with the kth level, $k = 1, 2, 3$, while $\Omega_{\rm R1}$ and $\Omega_{\rm R2}$ are the Rabi frequencies connected to the coupling between levels $|1\rangle$ and $|2\rangle$ and level $|3\rangle$. Here, for simplicity, we consider a symmetric Λ scheme, in which we have the same Rabi frequency $\Omega_0 = \Omega_{\rm R1} = \Omega_{\rm R2}$.

The master equation describing the behavior of the atomic ensemble under CPT interaction can be written as

$$\frac{\partial \hat{\rho}}{\partial t} + \hat{\Gamma}_{\rm rel}(t) = \frac{1}{i\hbar}[\mathcal{H}_{\rm CPT}, \hat{\rho}] + \hat{\Gamma}_{\rm exc}(t), \tag{39}$$

where the density operator $\hat{\rho}$ has the matrix elements $\rho_{j,k} = \langle j|\hat{\rho}|k\rangle$, $j, k = 1, 2, 3$. We recall that $\rho_k \equiv \rho_{k,k}$ represents the population of the kth level whereas $\rho_{j,k}$, with $j \neq k$, corresponds to the coherence between levels j and k.

In Eq. (39), $\hat{\Gamma}_{\rm rel}(t)$ represents the relaxation operator as expressed in the Bloch-Wagsness-Redfield theory (see Ref. [2] for details),

$$\hat{\Gamma}_{\rm rel}(t) = \frac{1}{2} \begin{pmatrix} \gamma_1\rho_1 & 2\gamma_2\rho_{1,2} & \Gamma^*\rho_{1,3} \\ 2\gamma_2\rho_{2,1} & \gamma_1\rho_2 & \Gamma^*\rho_{2,3} \\ \Gamma^*\rho_{3,1} & \Gamma^*\rho_{3,2} & 2\Gamma^*\rho_3 \end{pmatrix}, \tag{40}$$

and $\hat{\Gamma}_{\rm exc}(t)$ describes all the excitation process not induced by the coherent fields, namely,

$$\hat{\Gamma}_{\rm exc}(t) = \frac{1}{2} \begin{pmatrix} \Gamma^*\rho_3 + \gamma_1\rho_2 & 0 & 0 \\ 0 & \Gamma^*\rho_3 + \gamma_1\rho_1 & 0 \\ 0 & 0 & 0 \end{pmatrix}. \tag{41}$$

The coefficients γ_1 and γ_2 are the phenomenological relaxation rates of population and coherence in the ground state, respectively, and Γ^* is the relaxation rate of the excited state.

Assuming the rotating-wave and adiabatic approximations for the optical coherences and the absence of saturation of the optical transitions, in the steady-state conditions Eq. (39) has the solution [32]

$$\rho_1 = \rho_2 = \tfrac{1}{2}(1 - \rho_3), \tag{42a}$$

$$\rho_3 = \frac{2\Gamma_p}{\Gamma^*}\left(1 - \frac{2\Gamma_p(\gamma_2 + 2\Gamma_p)}{(\gamma_2 + 2\Gamma_p)^2 + (\Delta\omega)^2}\right), \tag{42b}$$

$$\rho_{1,2} = -\frac{\Gamma_p}{\gamma_2 + 2\Gamma_p + i\Delta\omega}, \tag{42c}$$

$$\rho_{1,3} = \rho_{2,3} = 0. \tag{42d}$$

Here $\Delta\omega$ is the two-photon Raman detuning defined as

$$\Delta\omega = (\omega_{\rm L1} - \omega_{\rm L2}) - \omega_{\rm A}. \tag{43}$$

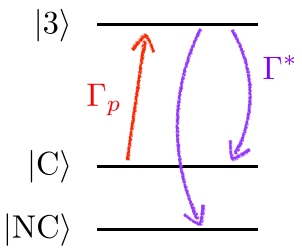

FIG. 13. The Λ scheme in terms of the coupled, $|\mathrm{C}\rangle$, and uncoupled, $|\mathrm{NC}\rangle$, states. This represents an optical pumping situation in which the atoms are pumped in the dark state. See the text for details.

Since the CPT approach is widely adopted in frequency standards operating with hot vapor cells, in previous equations we introduced the relaxation rates of the ground-state coherence and of the excited state, γ_2 and Γ^*, respectively, which take into account the decoherence processes occurring in the cell [2]. The laser pumping rate is given by $\Gamma_p = \Omega_0^2/2\Gamma^*$. The CPT physics can be better captured by describing the system using the so-called coupled, $|\mathrm{C}\rangle$, and uncoupled, $|\mathrm{NC}\rangle$, states [33]. In the case of the symmetric Λ scheme, they read

$$|\mathrm{C}\rangle = \frac{1}{\sqrt{2}}(|1\rangle + |2\rangle), \tag{44a}$$

$$|\mathrm{NC}\rangle = \frac{1}{\sqrt{2}}(|2\rangle - |1\rangle). \tag{44b}$$

It is possible to prove that the state $|\mathrm{NC}\rangle$ is not coupled to the radiation field [33]; thereafter, the following matrix element is identically null, namely,

$$\langle 3|\mathcal{H}_{\rm CPT}|\mathrm{NC}\rangle = 0, \tag{45}$$

whereas

$$\langle 3|\mathcal{H}_{\rm CPT}|\mathrm{C}\rangle = \frac{\hbar\Omega_0}{\sqrt{2}}. \tag{46}$$

Therefore, if the atom is in the $|\mathrm{NC}\rangle$ state it cannot be excited to level $|3\rangle$ and consequently no fluorescence signal can be generated: Whatever the initial condition is, the CPT Hamiltonian $\mathcal{H}_{\rm CPT}$ pumps all the atoms in the $|\mathrm{NC}\rangle$ state. The situation is represented in Figs. 12 and 13 in terms of the levels basis $\{|1\rangle, |2\rangle, |3\rangle\}$ and coupled and noncoupled basis $\{|\mathrm{C}\rangle, |\mathrm{NC}\rangle, |3\rangle\}$, respectively. This is an optical pumping process, where the $|\mathrm{NC}\rangle$ state is populated by the relaxation from the excited state $|3\rangle$ and from the depopulation pumping from level $|\mathrm{C}\rangle$, which is coupled to the radiation field [33].

We can use Eq. (44a) to calculate the matrix elements expressed in the basis of $|\mathrm{NC}\rangle$, $|\mathrm{C}\rangle$, and $|3\rangle$. In particular, we are interested in $\rho_{\rm NC} = \langle \mathrm{NC}|\hat{\rho}|\mathrm{NC}\rangle$, which gives the atomic population of the noncoupled state, and in $\rho_{\rm C} = \langle \mathrm{C}|\hat{\rho}|\mathrm{C}\rangle$. It is straightforward to see that

$$\rho_{\rm C} = \tfrac{1}{2}[1 - \rho_3 + 2\,\mathrm{Re}(\rho_{1,2})], \tag{47}$$

$$\rho_{\rm NC} = \tfrac{1}{2}[1 - \rho_3 - 2\,\mathrm{Re}(\rho_{1,2})], \tag{48}$$

which depend on the coherences $\rho_{1,2}$ between levels $|1\rangle$ and $|2\rangle$, and Eqs. (42) then yield

$$\rho_{\rm C} = \frac{1}{2}\left[1 - \frac{2\Gamma_p}{\Gamma^*}\left(1 + \frac{(\gamma_2 + 2\Gamma_p)(\Gamma^* - 2\Gamma_p)}{(\gamma_2 + 2\Gamma_p)^2 + (\Delta\omega)^2}\right)\right] \tag{49}$$

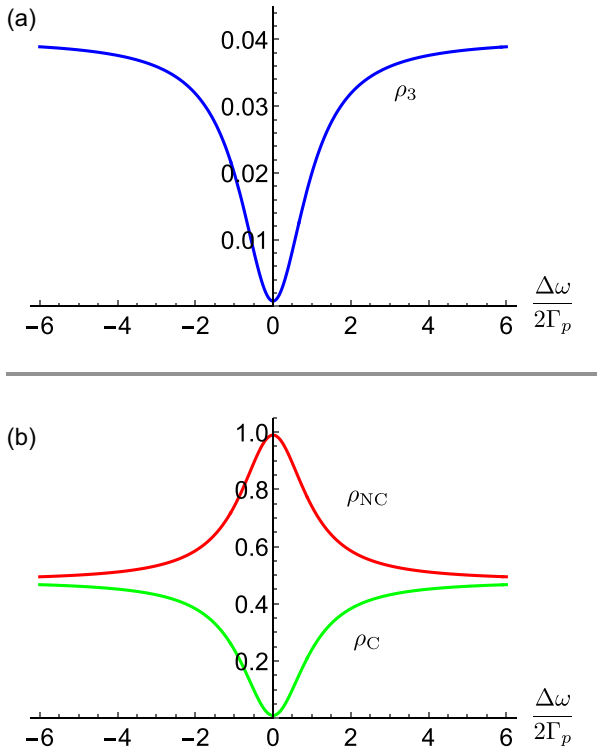

FIG. 14. Plots of (a) ϱ_3 and (b) $\rho_{\rm C}$ and $\rho_{\rm NC}$ as a function of the rescaled Raman detuning $\Delta\omega/2\Gamma_p$ (see the text for details). We consider the typical values $\gamma_2 = 400\ {\rm s}^{-1}$ and $\Gamma_p = 10^4\ {\rm s}^{-1}$.

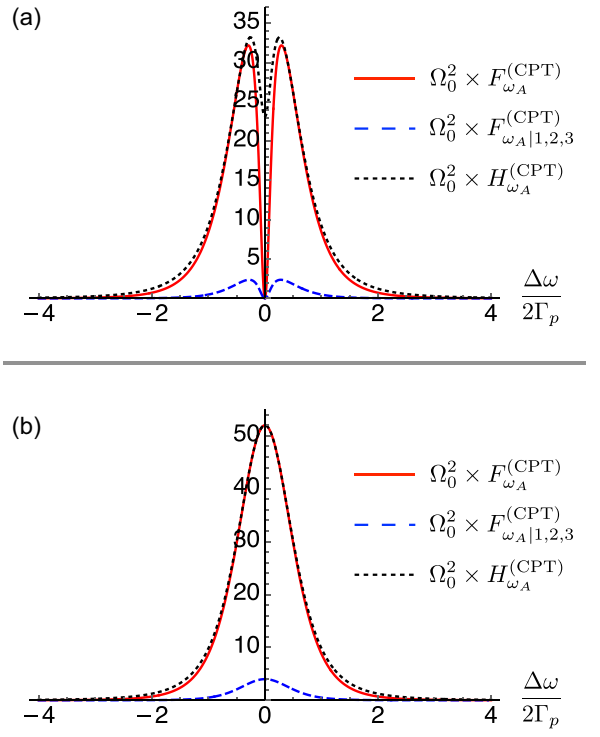

FIG. 15. (a) Plot of the Fisher information $F_{\omega_{\rm A}}^{\rm (CPT)}$ (red solid line) and $F_{\omega_{\rm A}|1,2,3}^{\rm (CPT)}$ (blue dashed line) as a function of $\Delta\omega/2\Gamma_p$. We set $\gamma_2 = 400\ {\rm s}^{-1}$ and $\Gamma_p = 10^4\ {\rm s}^{-1}$. (b) Same as in (a) but now we set $\gamma_2 \to 0$, that is, we neglect the relaxation of the ground-state coherence. The maximum is achieved at $\omega_{\rm L1} - \omega_{\rm L2} = \omega_{\rm A}$. See the text for details.

and

$$\rho_{\rm NC} = \frac{1}{2}\left[1 - \frac{2\Gamma_p}{\Gamma^*}\left(1 - \frac{(\gamma_2 + 2\Gamma_p)(\Gamma^* + 2\Gamma_p)}{(\gamma_2 + 2\Gamma_p)^2 + (\Delta\omega)^2}\right)\right]. \quad (50)$$

The behavior of ρ_3 and of $\rho_{\rm C}$ and $\rho_{\rm NC}$ versus the rescaled Raman detuning $\Delta\omega/2\Gamma_p$ is shown in Figs. 14(a) and 14(b), respectively. As expected, at resonance ($\Delta\omega = 0$) almost all the atomic population is pumped into the uncoupled state $|{\rm NC}\rangle$, that is, $\rho_{\rm NC} \approx 1$ and $\rho_{\rm C}, \rho_3 \approx 0$. Now scanning the frequency detuning $\Delta\omega$ across the resonance, one observes a dark resonance usually called a dark line [29].

First, we evaluate the Fisher information associated with the measurement of the population $\rho_l(\Delta\omega)$ of the level $|l\rangle$, with $l = {\rm C}, {\rm NC}, 3$, where we put in evidence the dependence on $\Delta\omega$ given in Eq. (43):

$$F_{\omega_{\rm A}}^{\rm (CPT)}(\Delta\omega) = \sum_{l={\rm C,NC},3} \rho_l(\Delta\omega)\left\{\partial_{\omega_{\rm A}} \ln[\rho_l(\Delta\omega)]\right\}^2. \quad (51)$$

Analogously, we can evaluate the Fisher information associated with the measurement involving the atomic energy states $|n\rangle$, with $n = 1, 2, 3$,

$$F_{\omega_{\rm A}|1,2,3}^{\rm (CPT)}(\Delta\omega) = \sum_{n=1,2,3} \rho_n(\Delta\omega)\left\{\partial_{\omega_{\rm A}} \ln[\rho_n(\Delta\omega)]\right\}^2. \quad (52)$$

Finally, due to Eq. (6) and by using Eqs. (42) we obtain the corresponding quantum Fisher information $H_{\omega_{\rm A}}^{\rm (CPT)}(\Delta\omega)$, whose analytic expression is rather cumbersome and it is not reported explicitly (see Appendix C for further details). We recall that, by definition, the quantum Fisher information does not depend on the particular basis chosen to describe the system. In Fig. 15 we plot $F_{\omega_{\rm A}|l}^{\rm (CPT)}$ as a function of $\Delta\omega/2\Gamma_p$: We can see that the maximum value of $F_{\omega_{\rm A}|l}^{\rm (CPT)}$ is similar to that obtained with the Rabi method (see Fig. 2). It is clear that the information gained by the measurement of the energy levels (blue dashed lines in the figure) is much less with respect to that retrieved by measuring the system in the coupled and uncoupled basis. Therefore, performing a measurement that involves coherences between the energy states $|1\rangle$ and $|2\rangle$, as the assessment of the density-matrix elements $\rho_{\rm C}$ and $\rho_{\rm NC}$, allows retrieving a higher Fisher information that, in the limit of very small relaxation rate γ_2 and at resonance ($\Delta\omega = 0$), reaches the maximum value given the quantum Fisher information, as highlighted in Fig. 15(b). Concerning the practical point of view, we point out that the maser approach represents a technique to detect the clock transition through the atomic coherence [17,34].

In Fig. 15(a) we can clearly see the presence of a dip at $\Delta\omega = 0$. If compared with the results from Rabi and Ramsey schemes in ideal conditions, where the Fisher information achieves the maximum at resonance, this result could sound odd. However, this follows from the very definition of the Fisher information and an analogous behavior emerges also in the Rabi and Ramsey schemes when the excitation probabilities do not reach 1 at resonance (see, for instance, the discussion at the end of Sec. II C and Fig. 11). In fact, while the derivative with respect to ω_A of all the elements ρ_l vanishes at resonance (there is a maximum or a minimum), as one

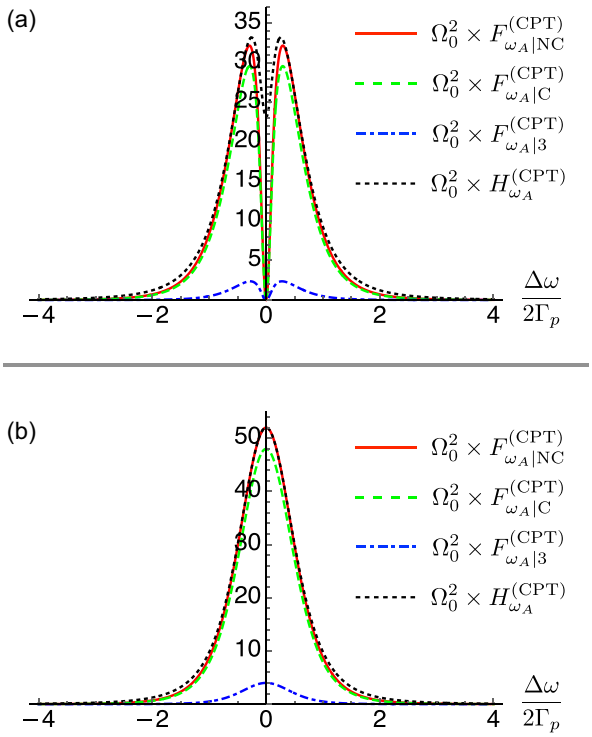

FIG. 16. (a) Plot of the single-level Fisher information $F^{(\mathrm{CPT})}_{\omega_\mathrm{A}|l}$, $l = \mathrm{C}, \mathrm{NC}, 3$, as a function of $\Delta\omega/2\Gamma_p$. We set $\gamma_2 = 400\ \mathrm{s}^{-1}$ and $\Gamma_p = 10^4\ \mathrm{s}^{-1}$. (b) Same as in (a) but now we set $\gamma_2 = 0$, that is, we neglect the relaxation of the ground-state coherence. As expected, the maximum is achieved at $\omega_{\mathrm{L}1} - \omega_{\mathrm{L}2} = \omega_\mathrm{A}$. See the text for details.

can see, for instance, in Fig. 14, in realistic conditions, none of these reaches 1 or 0 due to the presence of the relaxation of the ground-state coherence $\gamma_2 > 0$. Hence, the Fisher information vanishes and the quantum Fisher information displays a dip as well. Nevertheless, in actual experiments one can postprocess the data to "normalize" the measured quantities: The effect of this normalization is that the elements ρ_l now can reach 1 or 0 and the Fisher information no longer goes to zero at resonance but reaches a maximum, as expected. This can be seen in Fig. 15(b), where we neglected the relaxation of the ground-state coherence by setting $\gamma_2 = 0$, which is mathematically equivalent to suitably normalizing the matrix elements ρ_l, as one can see in particular from Eq. (42b). To better investigate the latter consideration, we can evaluate the Fisher and the quantum Fisher information associated with the measurement of just one of the states $|l\rangle$, with $l = \mathrm{C}, \mathrm{NC}, 3$ (analogous results are obtained addressing the energy-level states). Since now the measurement outcome is dichotomic, the Fisher information can be written as

$$F^{(\mathrm{CPT})}_{\omega_\mathrm{A}|l}(\Delta\omega) = \frac{[\partial_{\omega_\mathrm{A}}\rho_l(\Delta\omega)]^2}{\rho_l(\Delta\omega)[1-\rho_l(\Delta\omega)]}. \tag{53}$$

This makes evident that, at resonance, $F^{(\mathrm{CPT})}_{\omega_\mathrm{A}|l}$ vanishes since $\partial_{\omega_\mathrm{A}}\rho_l(0) = 0$ but $\rho_l(0)[1-\rho_l(0)] \neq 0$. If we set $\gamma_2 = 0$ or, equivalently, suitably normalize ρ_l as discussed above, we still have $\partial_{\omega_\mathrm{A}}\rho_l(0) = 0$ while now $\rho_l(0)[1-\rho_l(0)] = 0$ and the Fisher information reaches a maximum as shown in Fig. 16.

IV. CONCLUSION

In this paper we have investigated the ultimate quantum limits to the achievable uncertainty in the estimation of the transition frequency between two atomic levels.

We have used classical and quantum estimation theory to assess the three most important techniques in this field and proved that measuring the atomic population allows one to reach the minimum uncertainty. We have also shown that the Ramsey method beats both the Rabi and the CPT performance, confirming the current experimental evidence and justifying it within the framework of estimation and quantum estimation theory. In the case of the Rabi and Ramsey schemes, we investigated the effect of cavity coupling fluctuations: As expected, we have found a reduction of the actual value of the Fisher information and of its quantum counterpart, but our analysis has shown also that both of them drop to zero at resonance. The latter finding can be explained by considering that in the noiseless case the Cramér-Rao theorem cannot be applied at resonance, since here the statistical model changes its rank; however, when noise is considered, the rank of the statistical model remains always the same, leading to the found dip. A noiselesslike behavior can be restored by suitably postprocessing the data and rescaling the involved probabilities.

On the CPT side, we have found that the Fisher and the quantum Fisher information coincide for any value of the detuning $\Delta\omega = \omega_\mathrm{A} - \omega$, whereas for the Rabi and Ramsey methods, the quantum Fisher information is sensibly higher that the classical information only for nonzero values of $\Delta\omega$. We believe that this can foster new investigation in the search for different detection schemes able to reach that limit addressing also the coherences between the involved levels.

Even though the Ramsey method proves more effective in terms of Fisher information compared to Rabi and CPT techniques, it is nevertheless evident that some applications require very small devices (see, for example, Ref. [35]) for which coherent population trapping is particularly suited, since the clock transition is excited without the need of any microwave cavity. Also, in optical clocks the Rabi interaction is widely used, being much easier to implement than the Ramsey one. In this paper, however, we analyzed the three techniques from a statistical point of view, regardless of the implementation and practical uses of the clock. Our results may in turn foster further investigations beyond the well-established measurement schemes employed in atomic clocks. To this aim, in future investigations, we aim to examine the impact of physical noise sources (such as laser phase fluctuations and collision-induced decoherence) on the quantum Fisher information and its classical counterpart. This is particularly relevant in the context of the CPT scheme, where the clock signal is directly linked to atomic coherence.

ACKNOWLEDGMENTS

The authors acknowledge useful discussions with Marco Mancini in the early stage of this study. This work was partially supported by the Italian Ministry of Research and Next Generation EU via the PRIN-2022 project RISQUE

(Contract No. 2022T25TR3) and the NQSTI-Spoke2-BaC project QMORE (Contract No. PE00000023-QMORE).

DATA AVAILABILITY

There are no publicly available research data or software supporting this manuscript. Requests for further information or data should be sent to the authors.

APPENDIX A: DERIVATION OF EQ. (7)

A two-level atom, with transition frequency $\omega_{\rm A}$ between the ground ($|g\rangle$) and the excited ($|e\rangle$) states, is described by the Hamiltonian

$$\mathcal{H}_{\rm A} = \frac{\hbar\omega_{\rm A}}{2}\sigma_z, \tag{A1}$$

with $\sigma_z = |e\rangle\langle e| - |g\rangle\langle g|$ the Pauli matrix. We assume that the atom interacts with an oscillating electric field $\vec{E}(t) = E_0\vec{\varepsilon}_{\rm F}(e^{-i\omega t - i\phi} + e^{i\omega t + i\phi})$ inside a cavity, where E_0, ω, and $\vec{\varepsilon}_{\rm F}$ are the amplitude, the frequency, and the polarization of the field, respectively. If we assume the dipole approximation, the interaction between the atom and field can be described by the Hamiltonian

$$\mathcal{H}_{\rm int} = -\hat{D}\cdot\vec{E}(t), \tag{A2}$$

where $\hat{D} = \vec{d}\,(\sigma_+ + \sigma_-)$, with $\vec{d}$ the dipole transition moment, whereas $\sigma_+ = |e\rangle\langle g|$ and $\sigma_- = |g\rangle\langle e|$ are the raising and lowering operators, respectively.

Upon introducing the detuning $\Delta\omega = \omega_{\rm A} - \omega$, the total Hamiltonian can be written as

$$\mathcal{H} = \frac{\hbar\Delta\omega}{2}\sigma_z + \frac{\hbar\omega}{2}\sigma_z - \frac{\hbar\Omega_0}{2}(\sigma_+ + \sigma_-)(\mathrm{e}^{-i\omega t - i\phi} + \mathrm{e}^{i\omega t + i\phi}), \tag{A3}$$

where $\Omega_0 = 2\vec{d}\cdot\vec{\varepsilon}_{\rm F}E_0/\hbar$ is the Rabi frequency.

In the interaction picture with respect to the Hamiltonian

$$\mathcal{H}_0 = \frac{\hbar\omega}{2}\sigma_z, \tag{A4}$$

and performing the rotating-wave approximation, i.e., neglecting the terms proportional to $\mathrm{e}^{\pm 2i\omega t}$, Eq. (A3) becomes

$$\tilde{\mathcal{H}} = \frac{\hbar\Delta\omega}{2}\sigma_z - \frac{\hbar\Omega_0}{2}(\sigma_+\mathrm{e}^{-i\phi} + \sigma_-\mathrm{e}^{i\phi}) \tag{A5a}$$

$$= \frac{\hbar\Omega}{2}\vec{n}\cdot\vec{\sigma}, \tag{A5b}$$

where $\vec{\sigma} = (\sigma_x, \sigma_y, \sigma_z)$ is the vector of the Pauli matrices, $\Omega = \sqrt{\Omega_0^2 + (\Delta\omega)^2}$, and

$$\vec{n} = -\frac{1}{\Omega}(\Omega_0\cos\phi,\ \Omega_0\sin\phi,\ -\Delta\omega). \tag{A6}$$

Thereafter, the evolution operator (in the interaction picture) reads

$$\tilde{U}(\Omega_0; t) = \exp\left(-i\frac{\tilde{\mathcal{H}}}{\hbar}t\right) \tag{A7a}$$

$$= \begin{pmatrix} A_t(\Omega_0,\Delta\omega) & \mathrm{e}^{-i\phi}B_t(\Omega_0,\Delta\omega) \\ \mathrm{e}^{i\phi}B_t(\Omega_0,\Delta\omega) & A_t^*(\Omega_0,\Delta\omega) \end{pmatrix}, \tag{A7b}$$

with

$$A_t(\Omega_0,\Delta\omega) = \cos\left(\frac{\Omega t}{2}\right) - i\frac{\Delta\omega}{\Omega}\sin\left(\frac{\Omega t}{2}\right), \tag{A8a}$$

$$B_t(\Omega_0,\Delta\omega) = i\frac{\Omega_0}{\Omega}\sin\left(\frac{\Omega t}{2}\right). \tag{A8b}$$

In Eq. (A7b) we used the matrix formalism, where we considered as the basis

$$|g\rangle = \begin{pmatrix}0\\1\end{pmatrix}, \quad |e\rangle = \begin{pmatrix}1\\0\end{pmatrix}. \tag{A9}$$

Now, given the evolved state

$$|\psi(t)\rangle = \tilde{U}(\Omega_0; t)|g\rangle, \tag{A10}$$

if we choose the interaction time such that $\Omega_0 t = \pi$, namely, in the presence of a π pulse, the probability

$$p^{(e)}_{\omega_{\rm A}}(\omega) = |\langle e|\psi(t = \pi/\Omega_0)\rangle|^2 \tag{A11}$$

is equal to Eq. (7).

APPENDIX B: DERIVATION OF EQ. (13)

The evolution through the cavities is still described by the evolution operator given in Eqs. (A7), whereas the free evolution, in the interaction picture, is obtained by applying the operator

$$\tilde{U}_{\rm free}(t) = \exp\left(-i\frac{\Delta\omega t}{2}\sigma_z\right) \tag{B1a}$$

$$= \begin{pmatrix} \exp(-i\frac{\Delta\omega t}{2}) & 0 \\ 0 & \exp(i\frac{\Delta\omega t}{2}) \end{pmatrix}. \tag{B1b}$$

If the interaction time is τ for both cavities, the whole evolution can be written as

$$|\Psi_T(\tau)\rangle = \tilde{U}_2(\Omega_0;\tau)\tilde{U}_{\rm free}(T)\tilde{U}_1(\Omega_0;\tau)|g\rangle, \tag{B2}$$

where $\tilde{U}_k(\tau)$ is given in Eqs. (A7) with $\phi = \phi_k$ and, without loss of generality, we can assume $\phi_1 = 0$ and $\phi_2 = \phi$. Now if we now assume $\phi = 0$, $\tau = \pi/2\Omega_0$ (that is, a $\pi/2$ pulse), and $T = \kappa\tau$, the probability to find the atom in the state $|e\rangle$ after the whole evolution is

$$P^{(e)}_{\omega_{\rm A}}(\omega; T) = |\langle e|\Psi_T(\tau = \pi/2\Omega_0)\rangle|^2, \tag{B3}$$

which leads to Eq. (13).

APPENDIX C: DERIVATION OF THE QUANTUM FISHER INFORMATION FROM THE CPT DENSITY MATRIX

To evaluate the quantum Fisher information from Eq. (6) it is enough to find the eigenvectors $|\psi_l\rangle$ and the eigenvalues r_l, $l = 1, 2, 3$, of the density matrix $\hat{\rho}$ whose matrix elements are given by Eqs. (42). We have

$$|\psi_1\rangle = \frac{(1 - i\tilde{\Delta})|1\rangle + \sqrt{1 + \tilde{\Delta}^2}|2\rangle}{\sqrt{2(1 + \tilde{\Delta}^2)}}, \tag{C1}$$

$$|\psi_2\rangle = \frac{(1 + i\tilde{\Delta})|2\rangle - \sqrt{1 + \tilde{\Delta}^2}|1\rangle}{\sqrt{2}(1 + i\tilde{\Delta})}, \tag{C2}$$

$$|\psi_3\rangle = |3\rangle, \tag{C3}$$

where $|l\rangle$, $l = 1, 2, 3$, are the three energy levels of the atom and

$$\tilde{\Delta} = \frac{\Delta\omega}{\gamma_2 + 2\Gamma_p}. \tag{C4}$$

The corresponding eigenvalues $\hat{\rho}|\psi_l\rangle = r_l|\psi_l\rangle$ are

$$r_1 = \frac{1}{2}\left(1 - \frac{2\tilde{\Gamma}_p}{\sqrt{1+\tilde{\Delta}^2}} - r_3\right), \tag{C5}$$

$$r_2 = \frac{1}{2}\left(1 + \frac{2\tilde{\Gamma}_p}{\sqrt{1+\tilde{\Delta}^2}} - r_3\right), \tag{C6}$$

$$r_3 = \frac{2\Gamma_p}{\Gamma_*}\frac{\tilde{\gamma} + \tilde{\Delta}^2}{1+\tilde{\Delta}^2}, \tag{C7}$$

with

$$\tilde{\gamma} = \frac{\gamma_2}{\gamma_2 + 2\Gamma_p}, \quad \tilde{\Gamma}_p = \frac{\Gamma_p}{\gamma_2 + 2\Gamma_p}. \tag{C8}$$

Finally, the analytic expression of the quantum Fisher information can be retrieved through straightforward calculations from

$$H^{(\mathrm{CPT})}_{\omega_\Lambda}(\Delta\omega) = 2\sum_{m,n}\frac{\left|\langle\psi_n|\partial_{\omega_\Lambda}\hat{\rho}|\psi_m\rangle\right|^2}{r_n + r_m}, \tag{C9}$$

where $m, n = 1, 2, 3$. Due to its clumsy appearance, it is not reported here.

[1] F. Riehle, *Frequency Standards. Basics and Applications* (Wiley-VCH, Weinheim, 2004).

[2] J. Vanier and C. Audoin, *The Quantum Physics of Atomic Frequency Standards* (Hilger, Bristol, 1989).

[3] Y. Y. Jiang, A. D. Ludlow, N. D. Lemke, R. W. Fox, J. A. Sherman, L.-S. Ma, and C. W. Oates, Making optical atomic clocks more stable with 10^{-16} level laser stabilization, Nat. Photon. **5**, 158 (2011).

[4] M. S. Safronova, The search for variation of fundamental constants with clocks, Ann. Phys. (Berlin) **531**, 1800364 (2019).

[5] H. J. Metcalf and P. van der Straten, *Laser Cooling and Trapping* (Springer, Berlin, 1999).

[6] R. Wynands and S. Weyers, Atomic fountain clocks, Metrologia **42**, S64 (2005).

[7] A. D. Ludlow, M. M. Boyd, J. Ye, E. Peik, and P. O. Schmidt, Optical atomic clocks, Rev. Mod. Phys. **87**, 637 (2015).

[8] C. W. Helstrom, *Quantum Detection and Estimation Theory* (Academic Press, New York, 1976).

[9] S. L. Braunstein and C. M. Caves, Statistical distance and geometry of quantum states, Phys. Rev. Lett. **72**, 3439 (1994).

[10] M. G. A. Paris, Quantum estimation for quantum technology, Int. J. Quantum Inf. **07**, 125 (2009).

[11] I. I. Rabi, J. R. Zacharias, S. Millman, and P. Kusch, A new method of measuring nuclear magnetic moment, Phys. Rev. **53**, 318 (1938).

[12] N. F. Ramsey, Experiments with separated oscillatory fields and hydrogen masers, Rev. Mod. Phys. **62**, 541 (1990).

[13] N. F. Ramsey, *Molecular Beams* (Oxford University Press, Oxford, 1985).

[14] M. Gozzelino, S. Micalizio, C. E. Calosso, J. Belfi, A. Sapia, M. Gioia, and F. Levi, Realization of a pulsed optically pumped Rb clock with a frequency stability below 10^{-15}, Sci. Rep. **13**, 12974 (2023).

[15] N. Almat, M. Gharavipour, W. Moreno, F. Gruet, C. Affolderbach, and G. Mileti, Long-term stability analysis toward $<10^{-14}$ level for a highly compact POP Rb cell atomic clock, IEEE Trans. Ultrason. Ferroelect. Freq. Contr. **67**, 207 (2020).

[16] Q. Shen, H. Lin, J. Deng, and Y. Wang, Pulsed optically pumped atomic clock with a medium- to long-term frequency stability of 10^{-15}, Rev. Sci. Instrum. **91**, 045114 (2020).

[17] A. Godone, S. Micalizio, C. E. Calosso, and F. Levi, The pulsed rubidium clock, IEEE Trans. Ultrason. Ferroelect. Freq. Control **53**, 525 (2006).

[18] R. Bonifacio, S. Olivares, P. Tombesi, and D. Vitali, Model-independent approach to nondissipative decoeherence, Phys. Rev. A **61**, 053802 (2000).

[19] K. Beloy, Hyper-Ramsey spectroscopy with probe laser intensity fluctuations, Phys. Rev. A **97**, 031406(R) (2018).

[20] M. Hübner, Explicit computation of the Bures distance for density matrices, Phys. Lett. A **163**, 239 (1992).

[21] A. Lyons, G. C. Knee, E. Bolduc, T. Roger, J. Leach, E. M. Gauger, and D. Faccio, Attosecond-resolution Hong-Ou-Mandel interferometry, Sci. Adv. **4**, eaap9416 (2018).

[22] S. Blatt, J. W. Thomsen, G. K. Campbell, A. D. Ludlow, M. D. Swallows, M. J. Martin, M. M. Boyd, and J. Ye, Rabi spectroscopy and excitation inhomogeneity in a one-dimensional optical lattice clock, Phys. Rev. A **80**, 052703 (2009).

[23] W. J. Riley, *Handbook of Frequency Stability Analysis* (NIST, Boulder, 2008).

[24] S. Jefferts, J. Shirley, T. E. Parker, T. P. Heavner, D. M. Meekhof, C. Nelson, F. Levi, G. Costanzo, A. De Marchi, R. Drullinger, L. Hollberg, W. D. Lee, and F. L. Walls, Accuracy evaluation of NIST-F1, Metrologia **39**, 321 (2002).

[25] I. Goti, S. Condio, C. Clivati, M. Risaro, M. Gozzelino, G. A. Costanzo, F. Levi, D. Calonico, and M. Pizzocaro, Absolute frequency measurement of a Yb optical clock at the limit of the Cs fountain, Metrologia **60**, 035002 (2023).

[26] E. Arimondo, Coherent population trapping in laser spectroscopy, Prog. Opt. **35**, 257 (1996).

[27] R. Brewer and E. L. Hahn, Coherent two-photon processes: Transient and steady-state cases, Phys. Rev. A **11**, 1641 (1975).

[28] E. Arimondo and G. Orriols, Nonabsorbing atomic coherences by coherent two-photon transitions in a three-level optical pumping, Lett. Nuovo Cimento **17**, 333 (1976).

[29] G. Alzetta, A. Gozzini, L. Moi, and G. Orriols, An experimental method for the observation of R.F. transitions and laser beat resonances in oriented Na vapour, Nuovo Cimento B **36**, 5 (1976).

[30] J.-M. Danet, O. Kozlova, P. Yun, S. Guérandel, and E. Clercq, Compact atomic clock prototype based on coherent population trapping, EPJ Web Conf. **77**, 00017 (2014).

[31] D. V. Brazhnikov, S. M. Ignatovich, and M. N. Skvortsov, Light shift mitigation in microcell-based coherent-population-trapping atomic clocks in the field of two circularly polarized light beams, Phys. Rev. Appl. **21**, 054046 (2024).

[32] F. Levi, A. Godone, J. Vanier, S. Micalizio, and G. Modugno, Line-shape of dark line and maser emission profile in CPT, Eur. Phys. J. D **12**, 53 (2000).

[33] M. O. Scully and M. S. Zubairy, *Quantum Optics* (Cambridge University Press, Cambridge, 1997).

[34] A. Godone, F. Levi, S. Micalizio, and J. Vanier, Theory of the coherent population trapping maser: A strong-field self-consistent approach, Phys. Rev. A **62**, 053402 (2000).

[35] J. Kitching, Chip-scale atomic devices, Appl. Phys. Rev. **5**, 031302 (2018).